Sensors & Actuators: B. Chemical 276 (2018) 254–261

Contents lists available at ScienceDirect

Sensors and Actuators B: Chemical

journal homepage: www.elsevier.com/locate/snb

Plasmonic/magnetic graphene-based magnetofluoro-immunosensing platform for virus detection

Jaewook Lee[a], Kenshin Takemura[b], Enoch Y. Park[a,b,*]

[a] Research Institute of Green Science and Technology, Shizuoka University, 836 Ohya Suruga-ku, Shizuoka 422-8529, Japan
[b] Department of Applied Biological Chemistry, Graduate School of Integrated Science and Technology, Shizuoka University, 836 Ohya Suruga-ku, Shizuoka 422-8529, Japan

ARTICLE INFO

Keywords:
Plasmonic-magnetic graphene
Binary nanoparticle-decorated graphene
Magnetofluoro immunosensing
Plasmon resonance energy transfer based fluoro-immunosensing
Virus detection
Virus separation

ABSTRACT

Binary nanoparticles (NPs)-modified graphene has been spotlighted due to their multi-functionalities and various applications. In this study, Au and iron oxide NPs-decorated graphene was prepared as dual-functional plasmomagnetic graphene (PMGRP), which plays roles in both magnetic carrier and a plasmonic substrate, and was utilized for a magnetofluoro-immunosensing (MFIS) platform. As proof of concept study of plasmonic substrate effect, fluoro-immunosensing (FIS) for detection of influenza virus was demonstrated by using anti-hemagglutinin antibody (HA Ab)-modified PMGRP and quantum dot (QD). In the presence of the virus, the sandwich structure between PMGRP and QD was formed through HA Ab-virus conjugation, and the fluorescence of QD was depended on the virus concentration. Influenza virus A (H1N1) in deionized water was successfully detected with a detection limit of 7.27 fg/ml. When human serum was mixed into virus as a model of a biological sample, the target virus-captured PMGRP was separated from impurity by magnetic force and the MFIS was performed with QD assistance. This result shows that virus was successfully separated and detected without any interruption of impurities, thus PMGRP-based MFIS platform is a potential and promising system for detection of virus in complex biological samples.

1. Introduction

Plasmonic/magnetic hybrid nanomaterials have been spotlighted due to their multifunctional properties, such as the magneto-optical effect, surface-enhanced Raman scattering (SERS), plasmon resonance energy transfer (PRET), plasmonic coupling and enhanced electrical conductivity [1–6]. Based on these synergic functionalities, such assembled nanomaterials could be applied to various fields, for example, meta-materials, nano-optics, sensors, contrast agents, and nano-electronics [7–13]. Among several plasmonic-magnetic hybrid nanomaterials, metal/magnetic nanoparticles (NPs)-decorated carbon nanomaterials have attracted attention due to plasmonic/pi electrons and magnetic spin interactions. Indeed, a plasmonic coupling between metal nanoparticles on carbon nanomaterials could also occur due to pi electrons on carbon nanomaterials [14,15]. Thus, these hybrid nanomaterials have been used as plasmonic substrates, especially for sensing applications [16–19]. On the other hands, in order to conduct the on-site virus detection, the interference of impurities or biomolecules in the sample should be reduced because on-site sample was non-purified containing a lot of impurities with target virus, which reduces the sensing performance. Thus, to improve the sensing ability, a magnetic separation of target virus from the impurity is one of the effective sensing strategy.

In this study, Au/iron oxides (Au/IONPs)-decorated graphene was prepared as plasmonic/magnetic graphene (PMGRP), which is utilized for a target virus separator and a plasmonic substrate. We also used the PMGRP to detect a target virus through PRET-based magnetofluoro-immunosensing (MFIS) system. In addition, CdSeInS quantum dots (QDs) were used as a fluorescence indicator for a fluoro-immunosensing (FIS). In general, there is a PRET effect between the adjacent plasmonic material and a fluorescent material, which leads to enhanced fluorescence intensity [20–23]. Based on this phenomenon, in our previous works, Au/GRP and Au/carbon nanotube were applied as the plasmonic substrate for PRET-based FIS to detect influenza virus and *Mycobacterium tuberculosis*. And this sensing platform was successfully demonstrated via fluorescence enhancement effect based on target virus-mediated sandwich structure between Au/carbon nanomaterials and QDs [14,15].

MFIS was demonstrated with influenza virus A (New Caledonia/20/1999) (H1N1). Influenza viruses are classified into three types (A, B, C).

* Corresponding author.
E-mail address: park.enoch@shizuoka.ac.jp (E.Y. Park).

https://doi.org/10.1016/j.snb.2018.08.124
Received 20 March 2018; Received in revised form 24 August 2018; Accepted 24 August 2018
Available online 25 August 2018

Influenza virus A is the most common because it carries the infectious human pathogen and is highly diversified and easily mutated [24,25]. The pandemic influenza virus A (H1N1) occurred in 2009 and caused an outbreak of a respiratory infection that emanated from Mexico and spread globally to 191 countries [26,27].

To demonstrate MFIS, the PMGRP was synthesized through two steps: i) Graphene was mixed with Au^{3+} ions in deionized (DI) water by sonication, and ii) gallic acid-modified oxidizable IONPs (GA-IONPs) were added to the mixture and stirred for 3 h. During this step, Au^{3+} ions were reduced to Au NPs on the surface of graphene due to the reduction potential of GA-IONP [28]. In this case, the gallic acid has an anti-oxidant effect, so the GA-IONP can act as a reducing agent in this reaction [29]. At the same time, the GA-IONP also bound with graphene through pi-pi interactions between the aromatic groups of GA-IONP and graphene. This hybrid structure possesses plasmonic and magnetic properties and was designated as PMGRP.

2. Experimental section

2.1. Materials and instruments

Hydrogen tetrachloroaurate (III) (99.9%), gallic acid monohydrate (3,4,5-trihydroxy benzoic acid monohydrate), iron (III) chloride, iron (II) chloride tetrahydrate, L-cysteine, N-ethyl-N'-(dimethylaminopropyl) carbodiimide (EDC), N-hydroxysuccinimide (NHS), 25% ammonia solution and BSA were obtained from Sigma-Aldrich Co. LLC (Tokyo, Japan). Graphene flakes were purchased from Graphene Supermarket (Calverton, NY, USA). Three kinds of influenza viruses A (New Caledonia/20/99) (H1N1), (Netherlands/219/03) (H7N2) and (Hong-Kong/1073/99) (H9N2) were purchased from ProSpec-Tany TechnoGene Ltd. (Rehovot, Israel). Anti-hemagglutinin antibody (HA Ab) against influenza virus A (New Caledonia/20/99) (H1N1) HA (H1) and a mouse monoclonal Ab [B219 M] were purchased from Abcam Inc. (Cambridge, UK). Human serum was purchased from Sigma-Aldrich Co. LLC (Tokyo, Japan). Goat anti-mouse IgG-horseradish peroxidase was purchased from GE healthcare (Tokyo, Japan). Tetramethylbenzidine (TMBZ) was purchased from Dojindo (Kumamoto, Japan). To demonstrate magnetic separation, neodymium magnet (KENIS Ltd., Osaka, Japan) was used.

The plasmonic property of the PMGRP was measured using UV/Vis spectroscopy (Infinite® F500, TECAN, Ltd., Männedorf, Switzerland). The SERS effect of PMGRP was analyzed with an excitation wavelength of 532 nm by Raman spectroscopy (NRS-7100, JASCO, Tokyo, Japan). The functional groups of PMGRP were characterized by using FT-IR spectroscopy (FT-IR 6300, JASCO, Tokyo, Japan). The magnetic property of the PMGRP was measured from −30 kOe to + 30 kOe using a superconducting quantum interference device (SQUID, MPMS-XL7, Quantum Design, Inc., San Diego, CA, USA). The shape and surface morphologies of IONP, graphene, and PMGRP were observed using a transmission electron microscope (TEM, JEM-1400, JEOL, Tokyo, Japan), a high-resolution transmission electron microscope (HR-TEM, JEM-2100 F, JEOL, Tokyo, Japan), and a scanning electron microscope (SEM, JSM-6510LV, JEOL, Tokyo, Japan). The HA Ab conjugation with the PMGRP was confirmed by an enzyme-linked immunosorbent assay (ELISA) with a plate reader (Model 680, Bio-Rad, Hercules, CA, USA). The fluorescence of quantum dot (QD) and FIS was measured by using a filter-based multimode microplate reader (Infinite® F500; TECAN, Ltd, Männedorf, Switzerland).

2.2. Synthesis of PMGRP

Firstly, oxidizable GA-IONP was prepared as a reducing agent for Au NP decoration. Briefly, 1 mmol of iron chloride and 0.5 mmol of iron (II) chloride tetrahydrate were dissolved in 20 ml of DI water. Subsequently, 0.6 ml of 25% ammonia water was dropped into the mixture and stirred for 10 min for co-precipitation process to form the IONP. After that, 1.5 mmol of gallic acid powder was added into IONP solution and stirred for 30 min for 90 °C. After stirring process, GA-IONPs were precipitated with excess acetone and purified by a magnet separation.

PMGRP was prepared at room temperature in two steps. Five mg of graphene and 10 mg of hydrogen tetrachloroaurate (99.9%, 25 mmol) were mixed in 40 ml of DI water by sonication for 30 min. This Au ion and graphene mixture was added 1 ml of GA-IONP solution (1 mg/ml concentration in DI water) and then was vigorously stirred for 3 h. Finally, the PMGRP was separated by centrifugation and external magnetic field.

2.3. Antibody modification process and virus separation and MFIS test for virus detection

Influenza virus detection via PMGRP-based FIS was conducted with a 96-well plate for a preliminary study to confirm the role of the PMGRP as a plasmonic substrate. Firstly, in order to conjugate HA Ab on the surface of PMGRP, amine functionalization was carried out. One ml of cysteamine (0.03 M) was added into PMGRP (3 mg/ml) and this mixture was stirred for 1 h. During this reaction, the thiol group of cysteamine was attached on the surface of Au NP in PMGRP structure. After the reaction, amine group modified PMGRP was separated and purified by using external magnetic force and washed by using D.I water. Secondly, to fabricate plasmonic substrate, 50 µl of amine group modified PMGRP (2.5 mg/ml) was added into 96-well and magnetically deposited in each well plate and dried at room temperature. After that, 50 µl of EDC (1 mg/ml)/well and 50 µl of NHS (1 mg/ml)/well were added to the wells for HA Ab conjugation reaction. Fifty one ng/ml of HA Ab/well were added to the 96-well plate, shaken briefly 30 s and stayed overnight at 7 °C. After that, the 96-well plate washed 3 times using 200 µl of PBST (1 l of 0.1 M PBS + 5% Tween). After HA Ab conjugation process, HA Ab-PMGRP binding was confirmed by ELISA test. The sensitivity test was carried out with various concentrations of influenza virus from 1 fg/ml to 10 pg/ml. In this case, 100 µl of each concentration of virus was added into the mixture and shaken for 1 h. And then, 50 µl of QD (1 mg/ml) was dropped into the mixture to induce the virus-mediated sandwich structure for FIS. The fluorescence intensity of hybrid structure was measured with 450 nm excitation wavelength, and the maximum fluorescence intensity was collected at 614 nm emission wavelength for the calibration curve.

Influenza virus A (H1N1) in human serum was monitored through MFIS platform. Human serum is a mimic of complex biological matrices, containing iron 35–180 mg, cholesterol 110–210 mg, triglyceride 30–175 mg, glucose 60–140 mg, endotoxin < 10 EU, and hemoglobin 20 mg (Sigma–Aldrich, Louis, MO, USA). By mixing human serum and target virus, detection performance was investigated under conditions close to actual clinical samples. Various concentrations of the virus in the range of 0.1 pg/ml to 1000 pg/ml was added into 90 µl of human serum and its sensitivity test was carried out. Briefly, 0.2 mg/ml concentration of HA Ab-conjugated PMGRP was added into the influenza virus/human serum matrix and the mixture was shaken for 15 min for antibody-virus conjugation reaction. Virus subsequently conjugated HA Ab-PMGRP and was separated by external magnetic force for 3 min and the supernatant was removed. After washing process, 50 µl of HA Ab-conjugated QD (1 mg/ml) was added into the virus-PMGRP solutions to be monitored fluorescence intensity depending on the virus concentration. The fluorescence intensity was meadured with 450 nm excitation wavelength, and the maximum fluorescence intensity was collected at 614 nm emission wavelength for the calibration curve.

3. Results and discussion

3.1. Physicochemical property of PMGRP

The physicochemical properties of PMGRP have been characterized,

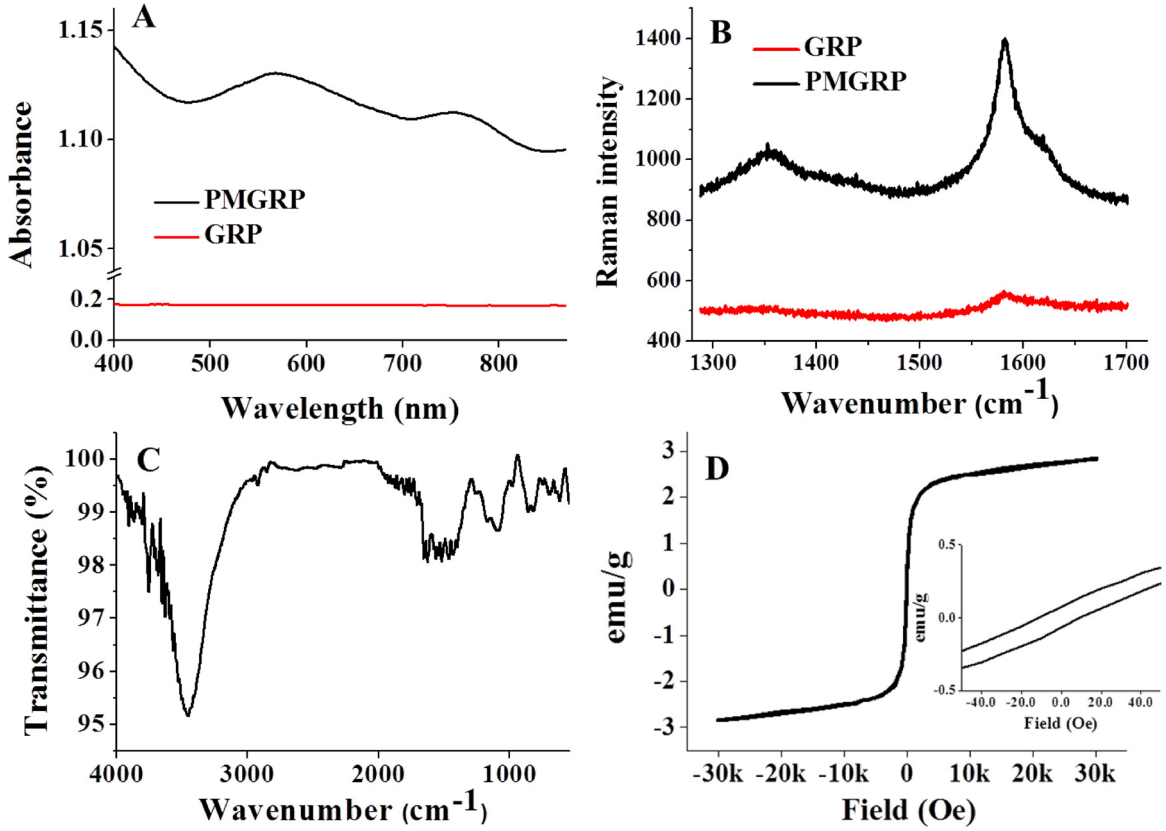

Fig. 1. Physicochemical characterization of graphene (GRP) and PMGRP: (A) UV/Vis spectrum for plasmonic absorbance, (B) Raman spectrum for SERS effect, (C) IR spectrum and (D) SQUID for magnetic properties.

including plasmonic and magnetic aspects. The plasmonic absorbance of PMGRP was measured by UV/Vis spectroscopy. A broad absorbance band appeared near 580 nm (Fig. 1A), which indicates that the size of Au NP on the graphene was polydisperse. In addition, the secondary absorbance band was shown around 755 nm. This absorbance was related with plasmonic coupling interaction between adjacent Au NPs on the GRP, and this effect was induced via pi electrons on the GRP [30]. The pi electrons were delocalized, so free electron movement occurred on the surface of GRP. And this electron movement caused the plasmonic coupling reaction between Au NPs, so it was assumed that GRP played a role as a mediator in the plasmonic coupling interaction. The similar phenomenon was also observed in Au NP-GRP and Au NP-CNT hybrid structures [14,15]. In addition, the SERS effect of PMGRP was characterized by Raman spectroscopy at an excitation wavelength of 532 nm (Fig. 1B). In this case, PMGRP and GRP were deposited on the Si wafer to measure the Raman spectrum of D band and G band to compare the intensity for SERS effect. The Raman intensity of PMGRP was 3 times higher than that of PMGRP due to the SERS effect. It was established that decoration of Au NP on the graphene contributed to the SERS effect which was induced through the electromagnetic mechanism based charge transfer between Au NP and GRP [31]. The D band of PMGRP was clearly observed at approximately 1355 cm^{-1}, and the G band was indicated at approximately 1582 cm^{-1}. In addition, a secondary band appeared at approximately 1618 cm^{-1}, because PMGRP was not a single layer but multiple layers stacked on the Si substrate by external magnetic force. The functional groups of PMGRP were analyzed by FT-IR spectroscopy, and its spectrum is shown in Fig. 1C. The aromatic group of PMGRP is seen at 1452 cm^{-1} – 1570 cm^{-1}. The alkane and alkene group in PMGRP appeared at approximately 2900 cm^{-1} and 3090 cm^{-1}, respectively. The carbonyl group of gallic acid was measured at approximately 1650 cm^{-1}, and the C–O vibration was characterized near 1090 cm^{-1}. Moreover, the Fe-O vibration was observed at approximately 600 cm^{-1}. The magnetic property of IONP and PMGRP was measured using a SQUID. In the case of IONP, magnetic hysteresis curve was clearly observed and depicted in Fig. S1. The remanence effect of IONP has indicated around -0.96 emu/g and 0.86 emu/g, and the coercive force was measured about -28.03 Oe and 28.05 Oe. And after decoration process, the remanence effect of PMGRP was indicated at approximately -0.07 emu/g and 0.07 emu/g according to the magnetic hysteresis curve of PMGRP (Fig. 1D). In addition, coercive force was analyzed at approximately 9.33 Oe, and -11.21 Oe, indicating that graphene possesses magnetic force after IONP decoration. In addition, the optical property of QD was characterized by UV/Vis spectroscopy and fluorescence spectroscopy. The absorbance λ_{max} of QD was indicated at approximately 380 nm, and the maximum fluorescence intensity of QD was estimated at 620 nm (Fig. S2) at the emission spectra of 450 nm.

3.2. Morphology of PMGRP

The morphology and shape of graphene were observed through a TEM. Graphene shows a smooth, clean surface (Fig. 2A). The size and structure of IONP were also observed at approximately 12 nm with a spherical shape (Fig. S3). After decoration on the surface of graphene, two different types of particles appeared and were well-dispersed on the surface of graphene; large, black particles indicates Au NP, and small, gray dots IONP (Fig. 2B and C). Because the electron density of the Au NP surface is higher than that of IONP, Au NP was darker than IONP. The size of Au NP was around 250 nm. The surface of PMGRP was also observed via SEM without ions or Pt sputtering. PMGRP possessed excellent electrical conductivity, so a hybrid structure was clearly exhibited with SEM without surface treatment. Large and white particles indicated Au NPs, and tiny, gray particles IONPs (Fig. 2D).

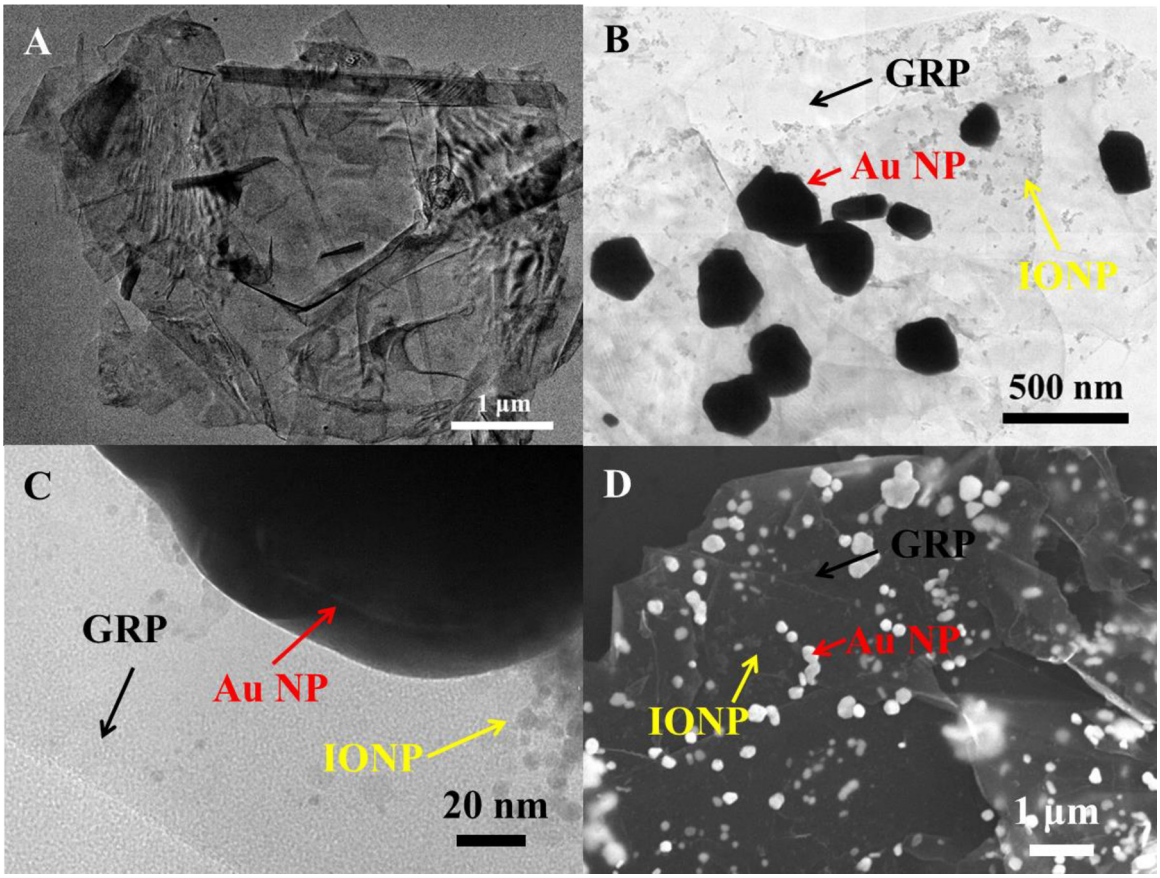

Fig. 2. TEM images of (A) graphene, (B) PMGRP (at low mag, × 20 k) and (C) PM-GRP (at high mag, × 150 k) and SEM image of (D) PMGRP.

3.3. Confirmation of plasmonic substrate effect of PMGRP via FIS test

Influenza virus detection was conducted through PMGRP-based FIS to confirm the plasmonic substrate function of PMGRP. The hybrid material was magnetically deposited in a 96-well plate to fabricate the plasmonic substrate. After deposition, an HA Ab against influenza A virus (New Caledonia/20/1999) (H1N1) HA (H1) was conjugated on the surface of amine-modified Au NPs on PMGRP through an EDC/NHS coupling reaction to capture the target virus. HA Ab was also conjugated on the surface of QD to develop the fluorescence, depending on the interaction with target virus. HA Ab conjugation on the surface of both PMGRP and QD was confirmed by an ELISA test (Fig. S4), indicating that HA Ab was successfully conjugated on the surface of PMGRP and QD via an EDC/NHS process.

When a target virus is present in this system, a sandwich structure between PMGRP and QD was assembled via HA Ab and virus interactions (Fig. 3A), and fluorescence intensity of QD (*FL*) was enhanced by the PRET effect. In this case, the virus size is around 100 nm, so the distance between PMGRP and QD was little far. However, the size of Au NP was large, and many Au NPs were attached on the surface of PMGRP which showed plasmonic coupling effect via pi electron. Not only Au NP on the GRP but also PMGRP itself played a role as the plasmonic substrate for energy transfer, and it means that the synergic effect of the plasmonic property was utilized for energy transfer. Thus, the distance issue of sandwich structure was overcome and enhancement was occurred. Moreover, the difference of enhanced *FL* (Δ*FL*) was correlated with the concentration of target virus [14,15]. The Δ*FL* was depended on the concentration of influenza virus (Fig. 3B). Based on this approach, the Δ*FL* with various concentrations of virus from 1 fg/ml to 10 pg/ml was collected at 618 nm to characterize the calibration curve and Δ*FL* was calculated by Equation 1 as below.

$$\triangle FL = FL_{with\ virus} - FL_0 \quad (1)$$

Where 0 the subscript of *FL* denotes *FL* value at 0 fg/ml of virus concentration. Through this calibration curve, a linear response was obtained with a correlation coefficient (R^2) of 0.9664 (Fig. 3C). The PMGRP-based FIS exhibited a good sensitivity performance, and the limit of detection of this system was estimated at approximately 7.27 fg/ml using a linear regression (Equation S1 in the SI). In addition, a selectivity test was conducted with 2% BSA, influenza viruses A (H7N2) and A (H9N2) at 10 ng/ml. Even a high concentration of other types of influenza virus was introduced into this system, and only fluorescence intensity highly increased at 10 ng/ml of H1N1 (Fig. 3D). Thus, the PMGRP-based FIS exhibited excellent performance in terms of specificity.

Virus detection was visualized after antibody and virus conjugation using a confocal microscope with an excitation wavelength of 405 nm. The PMGRP was magnetically deposited on the cover glass slide to fabricate the plasmonic substrate and modified with HA Ab. After that, 1 ng/ml of influenza virus A (H1N1) was introduced to induce a virus-mediated sandwich structure between PMGRP and QD. The QDs on the virus-HA Ab-PMGRP structure subsequently showed orange fluorescence spots on the surface of hybrid materials by using a confocal microscope. Thus, the virus can be visually monitored using hybrid nanomaterials (Fig. 4). On the other hands, the influenza virus used in this study (purchased from company) was observed and target separation process was monitored by using TEM. The round shape of influenza virus was observed (blue arrow in the image), and the size was less than 100 nm. Also, some impurities like protein structures (gray structures and small black dots) were also observed around the virus before separation process (Fig. S5A). However, after the virus was captured and isolated by PMGRP through external magnetic force, viruses were observed around the Au NP (Fig. S5B). It meant that target separation

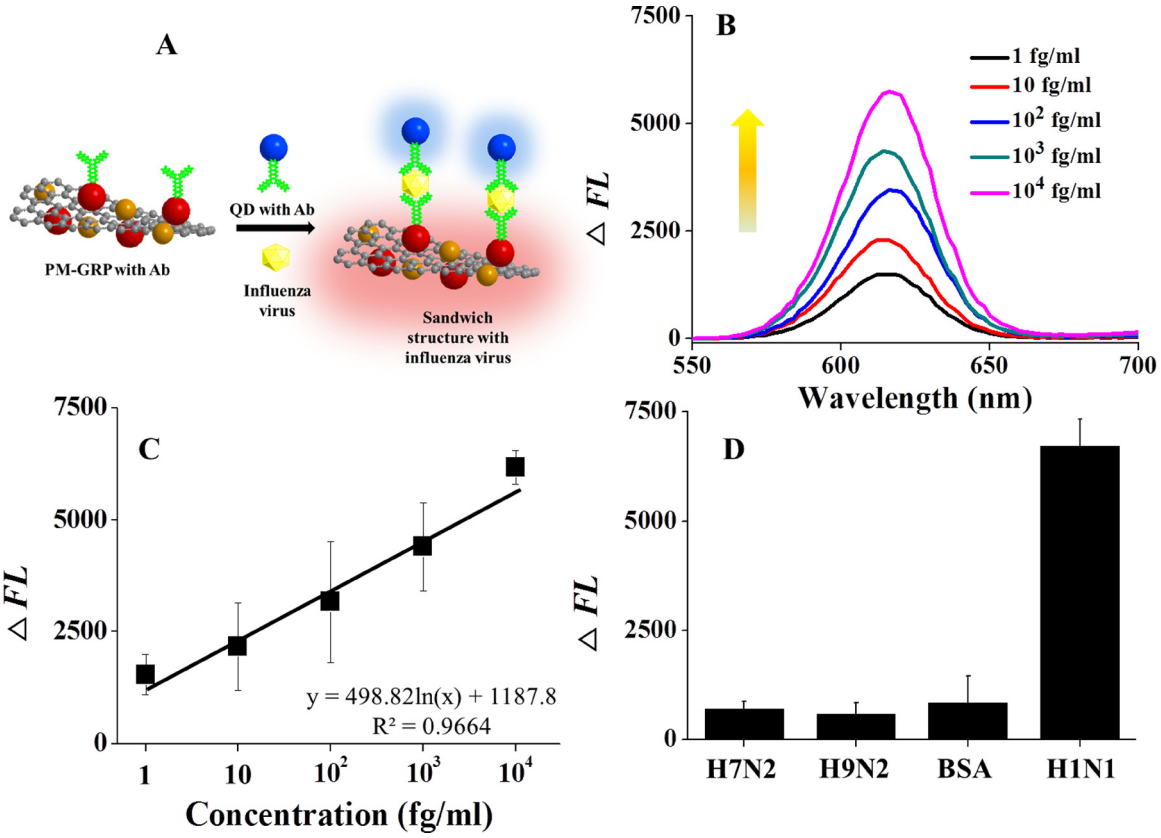

Fig. 3. Influenza virus detection performance with PMGRP-based FIS. (A) Schematic illustration of detection mechanism (not to scale), (B) monitoring of FL spectra depending on virus concentration, (C) calibration curve of ΔFL and virus concentration in the PMGRP-based on FIS results, and (D) selectivity test against other types of influenza virus.

process using PMGRP via magnetic force was successfully demonstrated.

3.4. Influenza virus detection via PMGRP-based MFIS platform

The influenza virus in impurities was detected by PMGRP-based MFIS, which has the magnetic separation of target virus from impurities and the plasmonic substrate for FIS. Firstly, the multi-functional PMGRP was added into the sample that was a mixture of target virus and impurities. During the mixing and shaking process, the target virus was bound to the HA Ab-conjugated PMGRP which was recovered from the supernatant containing impurities by the external magnetic force (Fig. 5). The target virus bound HA Ab-conjugated PMGRPs were replaced DI water of the same amount of the supernatant. Secondly, the HA Ab-conjugated QDs were added into the virus-bound HA Ab-conjugated PMGRP solution, and the QD-virus-PMGRP sandwich structure was induced. The Δ*FL* was depending on the concentration of target virus.

After magnetic separation process, the Δ*FL* was obviously monitored depending on the concentration of target virus (Fig. 6A). The Δ*FL* was correlated with the concentration of target virus in the mixture and was dependent on the virus concentration. As the control test, influenza virus in the human serum was detected using PMGRP without magnetic separation process in the virus concentration range from 0.1 pg/ml to 1000 pg/ml. The Δ*FL* was not clearly measured, and linearly response was not obtained depending on the concentration of virus (red circles in Fig. 6B). On the other hands, a linear response was obtained under magnetic separation process (black squares in Fig. 6B) with the limit of detection (LOD) of 6.07 pg/ml. It means that magnetic separation process successfully occurred and target virus was obviously detected

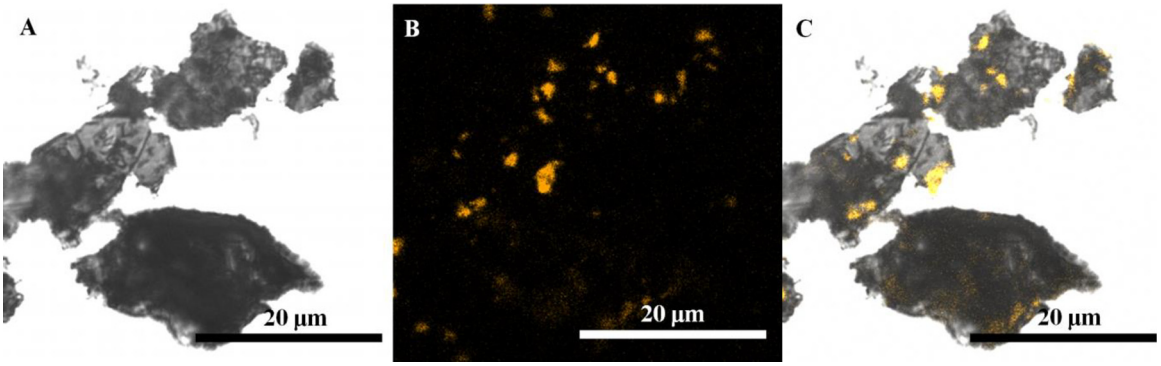

Fig. 4. Confocal microscopic fluorescence images after virus conjugation with PMGRP and QD via antibody and virus binding; (A) optical microscope image, (B) fluorescent image and (C) {(A) + (B)} merged image.

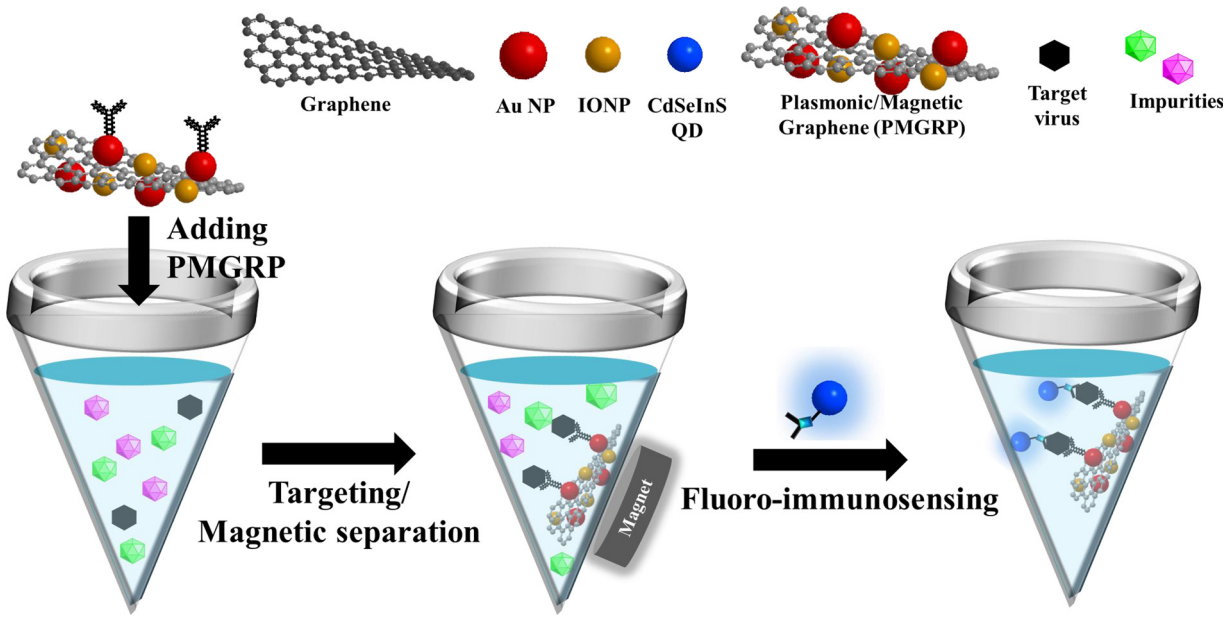

Fig. 5. Schematic illustration of target virus monitoring through PMGRP-induced magnetofluoro-immunosensing (MFIS) process (Not to scale).

by MFIS system. Compared with LOD in buffer condition detection, that in impurity-MFIS based detection was higher because the concentration window in each detection test was different. The slope of MFIS-based detection was 810.9, while it is 498.8 in DI water system. Correlation coefficient of MFIS-based detection was 0.97, while it is 0.91 in DI water system. These results indicate that detection performance was improved by magnetic separation, but statistical accuracy was lower compared to that of DI water system. This means that the impurities in sample still interfere the detection accuracy in the MFIS-based detection system.

Recently, various approaches for detection of influenza virus have been developed by using nanotechnology-based sensing systems [32], and MFIS system was compared with other researches (Table 1). In some of other cases, virus was monitored in pure environment without impurity, however in this case, virus in impurity mixed sample was detected. Even though the virus sample in this study was mixed with other biomolecule, interestingly, the LOD of this system is similar with them or lower than that of other detection systems. It meant that this system was regarded as a potential detection method for the virus in impurity mixed sample. Thus, multi-functional PMGRP-based MFIS process successfully demonstrated the detection of a target virus in a biological sample containing lots of impurities.

Table 1
Recent research comparison of influenza virus detection with various approaches.

Detection method	Target virus	LOD	Ref
Localized surface plasmon coupled fluorescence fiber-optic biosensor	H1N1	13.9 pg/ml	[33]
Integrated liquid core waveguides based microfluidic immunosensor	H3N2	1 pg/ml	[34]
	H5N1	80 pg/ml	[35]
ITO-TFT based biosensor			
Electrochemical immunosensor with magnetic separation process	H7N9	6.8 pg/ml	[36]
Magnetofluoro immunoassay	H1N1 in serum	6.07 pg/ml	This work

4. Conclusions

The PMGRP possesses plasmonic and magnetic effects that are the attractive function for virus detection. In the proof of concept of virus detection, this hybrid structure played a role in the plasmonic substrate for FIS system with the assistance of QD. Influenza virus in DI water was detected with the LOD of 7.27 fg/ml. Furthermore, this detection method showed high selectivity among various biomolecules. Influenza

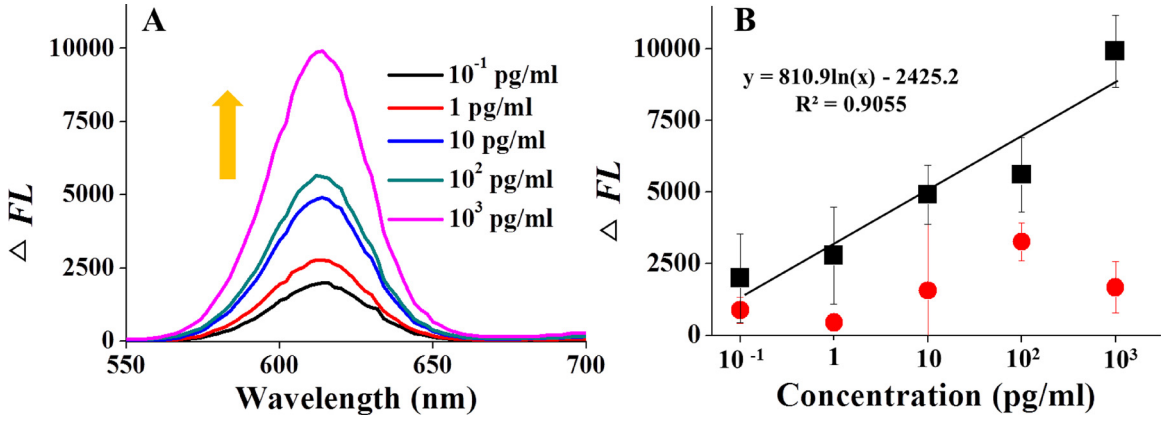

Fig. 6. Virus detection performance through MFIS. (A) spectra of the difference of FL, (B) sensitivity results depending on magnetic separation process and the concentration of influenza virus.

virus in human serum as a model of biological sample was separated from impurities by the magnetic property of PMGRP and was detected through QD-assisted FIS. Through PMGRP-based MFIS, influenza virus in human serum was detected with the LOD of 6.07 pg/ml, which is comparable to other studies. Particularly, compared with other cases which the virus was monitored without impurity, the excellent sensitivity of this system was shown. Thus, the PMGRP-based MFIS system is a potential biosensing and diagnostic platform for a complex biological sample.

Conflict of interest

The authors declare no competing financial interest.

Acknowledgments

This research was supported by the Japan Society for the Promotion of Science (JSPS) Postdoctoral Fellowship for Overseas Researchers (16F16361). This work was supported partly by the Bilateral Joint Research Project of the JSPS, Japan.

Appendix A. Supplementary data

Supplementary material related to this article can be found, in the online version, at doi:https://doi.org/10.1016/j.snb.2018.08.124.

References

[1] J. Lee, J. Lee, Magneto-optically active magnetoplasmonic graphene, Chem. Commun. (Camb.) 53 (2017) 5814–5817, https://doi.org/10.1039/C7CC01207A.
[2] J. Lee, S. Mulmi, V. Thangadurai, S.S. Park, Magnetically aligned iron oxide/gold nanoparticles decorated carbon nanotube hybrid structure as humidity sensor, ACS Appl. Mater. Interfaces 7 (2015) 15506–15513, https://doi.org/10.1021/acsami.5b03862.
[3] V. Yannopapas, A.G. Vanakaras, Strong magnetochiral dichroism in suspensions of magnetoplasmonic nanohelices, ACS Photonics 2 (8) (2015) 1030–1038, https://doi.org/10.1021/acsphotonics.5b00237.
[4] N. Maccaferri, X. Inchausti, A. García-Martín, J.C. Cuevas, D. Tripathy, A.O. Adeyeye, P. Vavassori, Resonant enhancement of magneto-optical activity induced by surface plasmon polariton modes coupling in 2D magnetoplasmonic crystals, ACS Photonics 2 (12) (2015) 1769–1779, https://doi.org/10.1021/acsphotonics.5b00490.
[5] F. Zou, H. Zhou, T.V. Tan, J. Kim, K. Koh, J. Lee, Dual-mode SERS-fluorescence immunoassay using graphene quantum dot labeling on one-dimensional aligned magnetoplasmonic nanoparticles, ACS Appl. Mater. Interfaces 7 (22) (2015) 12168–12175, https://doi.org/10.1021/acsami.5b02523.
[6] P.K. Jain, Y. Xiao, R. Walsworth, A.E. Cohen, Surface plasmon resonance enhanced magneto-optics (SuPREMO): faraday rotation enhancement in gold-coated iron oxide nanocrystals, Nano Lett. 9 (4) (2009) 1644–1650, https://doi.org/10.1021/nl900007k.
[7] J. Lee, K. Lee, S. Park, Environmentally friendly preparation of nanoparticle-decorated carbon nanotube or graphene hybrid structures and their potential applications, J. Mater. Sci. 51 (2016) 2761–2770, https://doi.org/10.1007/s10853-015-9581-0.
[8] J. Li, B. Arnal, C.-W. Wei, J. Shang, T.-M. Nguyen, M. O'Donnell, X. Gao, Magneto-optical nanoparticles for cyclic magnetomotive photoacoustic imaging, ACS Nano 9 (2) (2015) 1964–1976, https://doi.org/10.1021/nn5069258.
[9] S. David, C. Polonschii, C. Luculescu, M. Gheorghiu, S. Gáspár, E. Gheorghiu, Magneto-plasmonic biosensor with enhanced analytical response and stability, Biosens. Bioelectron. 63 (Supplement C) (2015) 525–532, https://doi.org/10.1016/j.bios.2014.08.004.
[10] J.M. Caicedo, O. Pascu, M. López-García, V. Canalejas, Á. Blanco, C. López, J. Fontcuberta, A. Roig, G. Herranz, Magnetophotonic response of three-dimensional opals, ACS Nano 5 (4) (2011) 2957–2963, https://doi.org/10.1021/nn1035872.
[11] P. Sharma, V. Bhalla, V. Dravid, G. Shekhawat, W. Jinsong, E.S. Prasad, C.R. Suri, Enhancing electrochemical detection on graphene oxide-CNT nanostructured electrodes using magneto-nanobioprobes, Sci. Rep. 2 (877) (2012), https://doi.org/10.1038/srep00877.
[12] B. Caballero, A. García-Martín, J.C. Cuevas, Hybrid magnetoplasmonic crystals boost the performance of nanohole arrays as plasmonic sensors, ACS Photonics 3 (2) (2016) 203–208, https://doi.org/10.1021/acsphotonics.5b00658.
[13] J. Lee, M. Morita, K. Takemura, E.Y. Park, A multi-functional gold/iron-oxide nanoparticle-CNT hybrid nanomaterial as virus DNA sensing platform, Biosens. Bioelectron. 102 (2018) 425–431, https://doi.org/10.1016/j.bios.2017.11.052.
[14] J. Lee, S.R. Ahmed, S. Oh, J. Kim, T. Suzuki, K. Parmar, S.S. Park, J. Lee, E.Y. Park, A plasmon-assisted fluoro-immunoassay using gold nanoparticle-decorated carbon nanotubes for monitoring the influenza virus, Biosens. Bioelectron. 64 (2015) 311–317, https://doi.org/10.1016/j.bios.2014.09.021.
[15] J. Lee, J. Kim, S.R. Ahmed, H. Zhou, J.-M. Kim, J. Lee, Plasmon-induced photoluminescence immunoassay for tuberculosis monitoring using gold nanoparticles decorated graphene, ACS Appl. Mater. Interfaces 6 (2014) 21380–21388, https://doi.org/10.1021/am506389m.
[16] N. Maccaferri, K.E. Gregorczyk, T. de Oliveira, M. Kataja, S. van Dijken, Z. Pirzadeh, A. Dmitriev, J. Akerman, M. Knez, P. Vavassori, Ultrasensitive and label-free molecular-level detection enabled by light phase control in magnetoplasmonic nanoantennas, Nat. Commun. 6 (2015) 6150, https://doi.org/10.1038/ncomms7150.
[17] J. Qin, Y. Zhang, X. Liang, C. Liu, C. Wang, T. Kang, H. Lu, L. Zhang, P. Zhou, X. Wang, B. Peng, J. Hu, L. Deng, L. Bi, Ultrahigh figure-of-merit in metal–insulator–metal magnetoplasmonic sensors using low loss magneto-optical oxide thin films, ACS Photonics 4 (6) (2017) 1403–1412, https://doi.org/10.1021/acsphotonics.7b00091.
[18] D.O. Ignatyeva, G.A. Knyazev, P.O. Kapralov, G. Dietler, S.K. Sekatskii, V.I. Belotelov, Magneto-optical plasmonic heterostructure with ultranarrow resonance for sensing applications, Sci. Rep. 6 (2016) 28077, https://doi.org/10.1038/srep28077.
[19] J. Lee, K. Takemura, E. Park, Plasmonic nanomaterial-based optical biosensing platforms for virus detection, Sensors 17 (10) (2017) 2332, https://doi.org/10.3390/s17102332.
[20] J. Lee, A.O. Govorov, J. Dulka, N.A. Kotov, Bioconjugates of CdTe nanowires and Au nanoparticles: plasmon − exciton interactions, luminescence enhancement, and collective effects, Nano Lett. 4 (12) (2004) 2323–2330, https://doi.org/10.1021/nl048669h.
[21] J. Lee, P. Hernandez, J. Lee, A.O. Govorov, N.A. Kotov, Exciton-plasmon interactions in molecular spring assemblies of nanowires and wavelength-based protein detection, Nat. Mater. 6 (4) (2007) 291–295, https://doi.org/10.1038/nmat1869.
[22] J. Lee, A.O. Govorov, N.A. Kotov, Nanoparticle assemblies with molecular springs: a nanoscale thermometer, Angew. Chem.-Int. Edit. 44 (45) (2005) 7439–7442, https://doi.org/10.1002/anie.200501264.
[23] K. Takemura, O. Adegoke, N. Takahashi, T. Kato, T.-C. Li, N. Kitamoto, T. Tanaka, T. Suzuki, E.Y. Park, Versatility of a localized surface plasmon resonance-based gold nanoparticle-alloyed quantum dot nanobiosensor for immunofluorescence detection of viruses, Biosens. Bioelectron. 89 (2017) 998–1005, https://doi.org/10.1016/j.bios.2016.10.045.
[24] M.C. Christman, A. Kedwaii, J. Xu, R.O. Donis, G. Lu, Pandemic (H1N1) 2009 virus revisited: an evolutionary retrospective, Infect. Genet. Evol. 11 (5) (2011) 803–811, https://doi.org/10.1016/j.meegid.2011.02.021.
[25] C.-H. Leung, H.-K. Tseng, W.-S. Wang, H.-T. Chiang, A.Y.-J. Wu, C.-P. Liu, Clinical characteristics of children and adults hospitalized for influenza virus infection, J. Microbiol. Immunol. Infect. 47 (6) (2014) 518–525, https://doi.org/10.1016/j.jmii.2013.06.002.
[26] M.P. Girard, J.S. Tam, O.M. Assossou, M.P. Kieny, The 2009 A (H1N1) influenza virus pandemic: a review, Vaccine 28 (31) (2010) 4895–4902, https://doi.org/10.1016/j.vaccine.2010.05.031.
[27] Ş. Özyer, S. Ünlü, Ş. Çelen, Ö. Uzunlar, S. Saygan, F.A. Su, M. Beşli, N. Danışman, L. Mollamahmutoğlu, Pandemic influenza H1N1 2009 virus infection in pregnancy in Turkey, Taiwan. J. Obstet. Gynecol. 50 (3) (2011) 312–317, https://doi.org/10.1016/j.tjog.2010.07.002.
[28] J. Lee, K. Takemura, C.N. Kato, T. Suzuki, E.Y. Park, Binary nanoparticle graphene hybrid structure-based highly sensitive biosensing platform for norovirus-like particle detection, ACS Appl. Mater. Interfaces 9 (32) (2017) 27298–27304, https://doi.org/10.1021/acsami.7b07012.
[29] J. Lee, H.Y. Kim, H. Zhou, S. Hwang, K. Koh, D.-W. Han, J. Lee, Green synthesis of phytochemical-stabilized Au nanoparticles under ambient conditions and their biocompatibility and antioxidative activity, J. Mater. Chem. 21 (35) (2011) 13316–13326, https://doi.org/10.1039/C1JM11592H.
[30] Y.H. Lee, L. Polavarapu, N. Gao, P. Yuan, Q.-H. Xu, Enhanced optical properties of graphene oxide–Au nanocrystal composites, Langmuir 28 (1) (2012) 321–326, https://doi.org/10.1021/la204047a.
[31] S. Sun, P. Wu, Competitive surface-enhanced Raman scattering effects in noble metal nanoparticle-decorated graphene sheets, Phys. Chem. Chem. Phys. 13 (47) (2011) 21116–21120, https://doi.org/10.1039/C1CP22727K.
[32] J. Lee, O. Adegoke, E.Y. Park, High-performance biosensing systems based on various nanomaterials as signal transducers, Biotechnol. J. (2018), https://doi.org/10.1002/biot.201800249 accepted article.
[33] Y.-F. Chang, S.-F. Wang, J.C. Huang, L.-C. Su, L. Yao, Y.-C. Li, S.-C. Wu, Y.-M.A. Chen, J.-P. Hsieh, C. Chou, Detection of swine-origin influenza A (H1N1) viruses using a localized surface plasmon coupled fluorescence fiber-optic biosensor, Biosens. Bioelectron. 26 (3) (2010) 1068–1073, https://doi.org/10.1016/j.bios.2010.08.060.
[34] B.C. Heinze, J.R. Gamboa, K. Kim, J.-Y. Song, J.-Y. Yoon, Microfluidic immunosensor with integrated liquid core waveguides for sensitive Mie scattering detection of avian influenza antigens in a real biological matrix, Anal. Bioanal. Chem. 398 (6) (2010) 2693–2700, https://doi.org/10.1007/s00216-010-4201-y.
[35] D. Guo, M. Zhuo, X. Zhang, C. Xu, J. Jiang, F. Gao, Q. Wan, Q. Li, T. Wang, Indium-tin-oxide thin film transistor biosensors for label-free detection of avian influenza virus H5N1, Anal. Chim. Acta 773 (2013) 83–88, https://doi.org/10.1016/j.aca.2013.02.019.
[36] Z. Wu, C.-H. Zhou, J.-J. Chen, C. Xiong, Z. Chen, D.-W. Pang, Z.-L. Zhang, Bifunctional magnetic nanobeads for sensitive detection of avian influenza A (H7N9) virus based on immunomagnetic separation and enzyme-induced metallization, Biosens. Bioelectron. 68 (2015) 586–592, https://doi.org/10.1016/j.bios.2015.01.051.

Jaewook Lee is current researcher in Research Institute of Green Science and Technology, Shizuoka University. He received his BS degree in chemistry in 2007 and MS degree in Analytical chemistry in 2009 from Dongguk University, Korea. Dr. Lee earned his Ph.D. degree in Nano Fusion Technology from Pusan National University. His current research interest includes synthesis of multi-functional nanomaterials and sensor applications. He has also interested in nanoparticles decorated carbon nanomaterials for nano-optics, and surface modification of nanocomposites for biocompatibility and biodegradability in nano bio-medical applications.

Kenshin Takemura is currently a graduate student in Graduate school of Integrated Science and Technology, Shizuoka University. He received his BS degree in 2016 and MS degree in Applied Biological Chemistry in 2018 from Shizuoka University, Japan. Mr. Takemura is studying for his PhD degree in Nanobiotechnology of Shizuoka University. His current research interest includes synthesis of functional nanoparticles and biosensor applications. He is also interested in localized surface plasmon resonance of nanocomposites for biosensing application.

Enoch Y. Park is currently a professor in Research Institute of Green Science and Technology, Shizuoka University. He received his MS degree in Korea Advanced Institute of Science and Technology in 1982, and Ph.D. degree in a major of Chemical Engineering from the University of Tokyo, Japan in 1990, and worked as assistant professor in the department of chemical engineering Nagoya University for two years. He is currently interested in preparation and engineering of nanobiomaterials such as virus-like particles. Also, he is interested in the expression of eukaryotic proteins in silkworm larvae and their applicability on biological detection of molecules.